Mesoporous doxorubicin-loaded polydopamine nanoparticles coated with platelet membrane suppress tumor growth in a murine model of human breast cancer

Dandan Ren[a], Gareth R. Williams[b], Yanyan Zhang[a], Rong Ren[a], Jiadong Lou[a] and Li-Min Zhu[a]*

[a] College of Chemistry, Chemical Engineering and Biotechnology, Donghua University, Shanghai, 201620, China

[b] UCL School of Pharmacy, University College London, 29-39 Brunswick Square, London, WC1N 1AX, UK

*Corresponding author: lzhu@dhu.edu.cn (Li-Min Zhu)

ABSTRACT: Bringing together photothermal therapy and chemotherapy (photothermal-chemotherapy, PT-CT) is a highly promising clinical approach, but requires the development of intelligent multi-functional delivery vectors. In this work, we prepared mesoporous polydopamine nanoparticles (MPDA NPs) loaded with the chemotherapeutic drug doxorubicin (DOX). These NPs were then coated with the platelet membrane (PLTM). The coated MPDA NPs are spherical and clearly mesoporous in structure. They have a particle size of approximately 184 nm and pore size of ca. 45 nm. The NPs are potent photothermal agents and efficient DOX carriers, with increased rates of drug release observed *in vitro* in conditions representative of the tumor microenvironment. The NPs are preferentially taken up by cancer cells, but not by macrophage cells, and while cytocompatible with healthy cells are highly toxic to cancer cells. An *in vivo* murine model of human breast cancer revealed that the NPs can markedly slow the growth of a tumor (ca. 9-fold smaller after 14 days' treatment), have extended pharmacokinetics compared to free DOX (with DOX still detectable in the bloodstream after 24h when the NPs are applied), and are highly targeted with minimal off-target effects on the heart, liver, spleen, kidney and lungs.

KEY WORDS: Mesoporous polydopamine; Platelet membrane; Combination therapy; Cancer therapy; Drug delivery system

INTRODUCTION

In recent years, extensive research into combining chemotherapy with near-infrared (NIR)-induced photothermal therapy (PTT) has been performed, with the aim of enhancing the effect of cancer therapies [1, 2]. This is often achieved by loading photothermal agents such as indocyanine green (ICG) [3, 4], chlorin e6 (Ce6)[5], and IR780 iodide[6] into drug-containing nano-carrier systems. There is however a drawback with such formulations, because the preparation methods are complex

and time consuming, while in addition loading the PTT agent may change the physical properties and/or reduce the drug loading of the materials[7]. Another approach is to prepare nano-carriers from materials with inherent PTT conversion ability, such as carbon-based nanomaterials[8], precious metals[9], or black phosphorus[10]. However, again the preparation process is usually complex, often requires harsh and dangerous reaction conditions, and there are risks of biological toxicity[11].

To overcome these challenges, a PTT material with high *in vivo* biocompatibility is required. Polydopamine (PDA) has attracted much attention to this end[12]. Dopamine is a natural melanin, and is widely distributed as a hormone in the human body. Dopamine can be self-assembled by oxygen polymerization under alkaline conditions to yield PDA[13]. PDA has excellent biocompatibility, offers the possibility for surface functional modification, acts as an NIR PTT agent[14-16], and is pH-responsive [17]. In 2007, Lee and co-workers first reported a PDA coating[18], and since then many researchers have used this method to endow a carrier with PTT properties[19-21]. However, when used as a coating, only a small proportion of the mass of the nanoparticle comprises PDA, which can hamper functional performance and biodegradability[22]. Coating also increases the final particle size and reduces the drug loading[23].

In recent years, many studies have therefore used PDA to prepare nanoparticles directly[24], ameliorating many of the above problems. Using trimethylbenzene as a template can lead to the formation of PDA particles with a mesoporous structure [25]. Mesoporous PDA (MPDA) particles have advantages of a large surface area[26-29] and high pore volume[22, 30-32]. Further, the pore size and particle size can be adjusted [33, 34].

Beyond the drug loading and functional performance of a nanoscale anticancer drug delivery system, it is also necessary to consider its fate in vivo. Common challenges include biological

adhesion, non-specific uptake of particles by healthy tissues, and phagocytosis by immune cells (e.g. macrophages)[35]. The enhanced permeability and retention (EPR) effect [36] helps the formulation to accumulate in cancerous cells via passive targeting, but has rather low efficiency. Active targeting is a more effective approach, [27] and is commonly achieved by making specific modifications to the surface of the carriers, adding ligands for receptors over-expressed on cancer cells (e.g. folic acid[37], antibodies[38], or targeting peptides[39]).

Surface modifications can also help to avoid the loss of nano-carriers from the blood circulation. Appropriate functionalization moieties for this purpose include polyethylene glycol and hyaluronic acid [40]. Unfortunately, the ability of such chemical modification to increase the blood circulation time of nano-carriers is often limited [41], and biomimetic approaches are emerging as potentially more powerful [42]. Here, a cell membrane is used to directly coat a nanoparticle. This has the advantages of a simple preparation method, biocompatibility, effective targeting, and the ability to avoid phagocytosis in vivo[43].

There are a range of proteins present in the cell membrane which can impart a carrier with the outer appearance of a host cell. In one of the earliest reports in this field, applying a red blood cell membrane coating to nanoparticles was found to increase the elimination half-life to 40 h, markedly longer than with a polyethylene glycol modification (15.8 h)[44]. Nanoparticles (NPs) wrapped in a leukocyte membrane can actively target tumor cells[45] and prevent nanoparticles from being cleared by white blood cells in vivo[46]. Particles wrapped in a cancer cell membrane can actively target homologous cancer cells[47]. Platelet cells have attracted particular attention for biomimetic coating applications. These cells comprise an important part of mammalian blood, playing a key role in hemostasis after vascular injury[48]. Platelets can also interact with macrophages through their CD47

membrane proteins, enabling them to avoid phagocytosis[49]. Furthermore, the presence of P-selectin on the platelet membrane enables coated NPs to bind to CD44, which is overexpressed on breast cancer cells. Thus, platelet membrane-coated nanoparticles can actively target tumor sites[50].

Here, we explore a strategy for the development of biomimetic nanoparticles using the platelet membrane and MPDA. The aim is to prepare an efficient nano-drug delivery system with high biocompatibility, low toxicity, active targeting, low immunogenicity and potent PTT properties. The chemotherapeutic doxorubicin (DOX) was incorporated into the particles. DOX has a broad-spectrum killing effect on most cancer cells, acting by inhibiting DNA and RNA synthesis. It is thus a potent chemotherapeutic, and its inclusion in our NPs should permit them to provide synergistic PTT-chemotherapy (Figure 1).

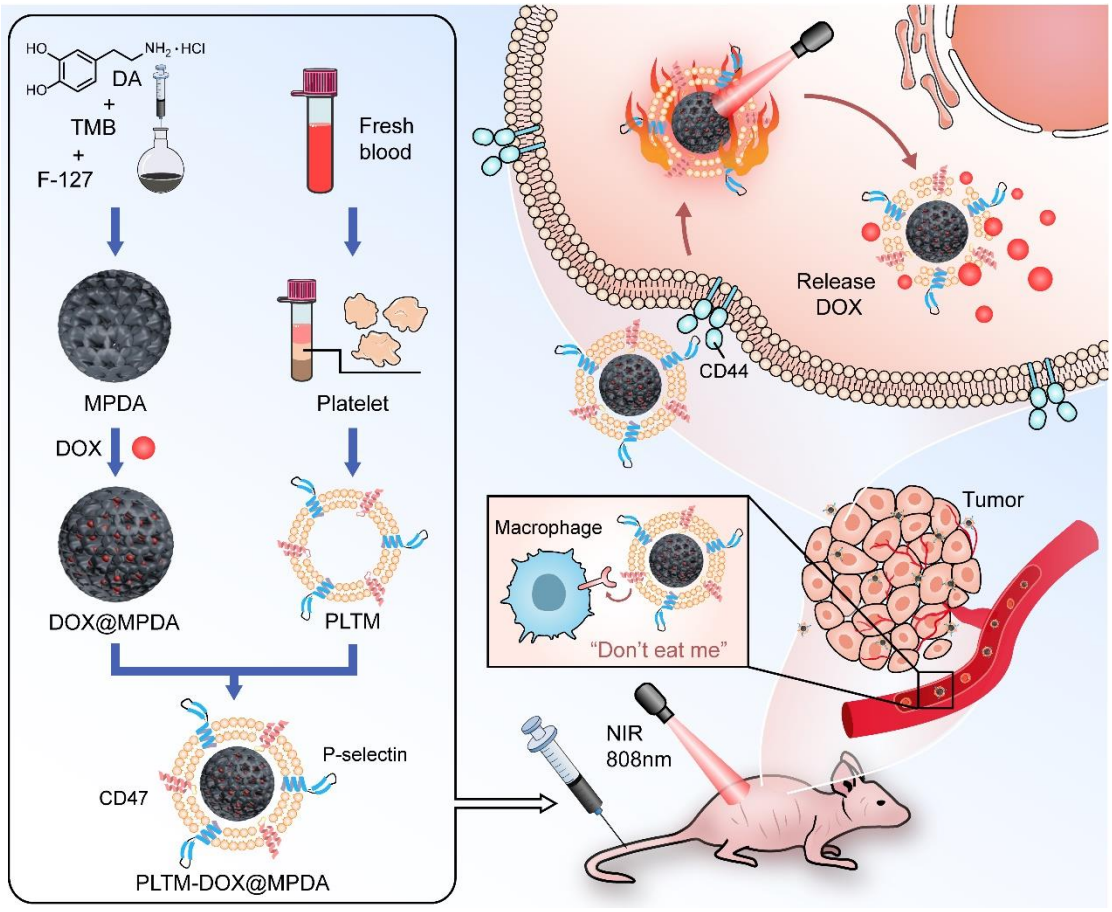

Figure 1. The synthetic approach used to develop anti-tumor NPs in this work.

EXPERIMENTAL SECTION

Preparation of MPDA NPs

Firstly, 1 g of F127 and 0.5 g of DA·HCl were dissolved in ethanol/water (50% v/v; 90 mL). The solution was stirred for 3 h at 1000 rpm at room temperature. 1.5 mL of TMB was then added drop-by-drop and the resultant mixture subjected to a 5 min sonication. The resultant mixture was stirred for another 30 minutes, before 5 mL of ammonia was added reaction allowed to continue for 3 h. Finally, the mixture was washed with ethanol three times and centrifuged to collect the product (13000 rpm, 10 min). This was freeze-dried at -45 ℃ for 48 h.

Preparation of DOX@MPDA

0.3 g of MPDA NPs was added to 10 mL of PBS, and 0.1 g of DOX was rapidly added to the MPDA suspension. After stirring at 300 rpm for 24 h, the suspension was centrifuged at 13000 rpm to sediment the MPDA NPs, which were collected and dispersed in 10 mL PBS. The supernatant was recovered and the residual DOX concentration was determined using UV-vis analysis. Loading content and encapsulation efficiency were calculated as follows:

Loading content = mass of loaded drug / total mass of formulation × 100%

Encapsulation efficiency = mass of drug in NPs / mass of drug in feedstock ×100%

Preparation of PLTM-DOX@MPDA

Blood was collected in anticoagulant tubes with sodium citrate from the jugular vein of nude mice. Blood (5 mL) was transferred into centrifuge tubes and layered above peripheral blood platelet separation medium. Following the manufacturer's instructions, the tube was subjected to centrifugation (18,000 rpm, 4 ℃, 20 min). The supernatant was then recovered and the platelet flocculent precipitate washed with 5 mL of PBS three times. The final platelet flocculent was transferred to 5 mL of PBS (pH=7.4; supplemented with 2 mM protease inhibitors and 1 mM EDTA),

and frozen at -80 ℃. The supernatant was then brought to room temperature and allowed to thaw slowly. This entire freeze-thaw process was repeated thrice. Finally, the material was sonicated (40 kHz, 100 W,) for 5 min to obtain a suspension of PLTM fragments.

To coat the NPs, 2 mL of DOX@ MPDA NPs in PBS (2 mg/mL) was combined with 200 μL of PLTM suspension, and the mixture subjected to sonication (40 kHz / 80 W for 4 min and 40 kHz / 100 W for 1 min). This resulted in PLTM-DOX@MPDA NPs, which were stored at 4 ℃.

Photothermal properties and in vitro drug release.

The temperature changes of PLTM-DOX@MPDA NP suspensions at different concentrations were recorded over 5 minutes of 808 nm NIR laser irradiation at a power density of 1.5 W cm^{-2}. Experiments were also performed at different power densities. The thermal stability of the NPs was ascertained by irradiating them five times with a laser (808 nm, 1.5 W cm^{-2}). The temperature of the PLTM-DOX @MPDA NPs suspension was determined using a digital thermometer, and images recorded on a thermal imaging camera (FLIR A300, Pumeng Technology, Shanghai, China). The photothermal conversion efficiency (PTCE) was calculated using the equation:

$$\eta = hS(T_{max}-T_{am})-Q_0 / I(1-10^{-A808})$$

S and h respectively correspond to the surface area of the container and the heat transfer coefficient. T_{max} is the equilibrium temperature, while T_{am} represents the ambient temperature. Q_0 is the heat absorption of the cell, is the laser power density (250 mW), and A_{808} the absorbency of the nanomaterials at 808 nm.

For DOX release studies, 2 mL of 1 mg/mL PLTM-DOX@MPDA NPs suspensions in PBS (pH 5.5 or 7.4) were sealed in a dialysis bag (MWCO = 7000 Da) and immersed in a large test tube filled with 18 mL PBS (pH 7.4 or 5.0) at 37 °C in a constant temperature shaker Periodically, 1 mL

of the external PBS buffer was removed for analysis, and fresh preheated buffer at the same pH added to maintain a constant volume in the release vessel. The amount of DOX released was analyzed using UV-vis spectroscopy (λ_{max} = 480 nm). All experiments were performed in triplicate.

Western blotting

The presence of platelet membrane proteins in PLTM-DOX@MPDA NPs was ascertained by western blotting. PLTM-DOX@MPDA NPs and the platelet membrane were first normalized to the same total protein concentration, determined with the aid of a Pierce BCA protein analysis kit. Proteins were extracted using a membrane protein extraction kit and the resultant solution (60 μL) was separated by SDS-PAGE (polyacrylamide gel electrophoresis), before being transferred to a polyvinylidene fluoride (PVDF) membrane and soaked in blocking solution (5% skimmed milk). Soaking proceeded at room temperature for 2 hours. Mouse anti-human CD41, mouse anti-human CD47 and P-selectin primary antibodies were then added, and the plate incubated overnight at 4 °C. After incubation, it was washed with 50 mL of PBS containing 0.05% v/v Tween 20. Goat anti-rat HRP (10 mL) coupled secondary antibodies were applied and the membrane incubated at room temperature for a further 2 h. SRX-101A Film Processor (Konica Minolta) and Premium autoradiography Films (Thomas Scientific (1141J52) were used for developing.

Characterization

A JEM 1200EX instrument (JEOL, Tokyo, Japan) was employed to collect transmission electron microscopy (TEM) images. IR spectra were obtained on a Nicolet Nexus 670 spectrometer (Thermo Fisher, Waltham, MA, USA), and UV-vis spectra on a UV-3600 spectrophotometer (Shimadzu, Tokyo, Japan). Dynamic light scattering (DLS) data were obtained with the aid of a Brookhaven Instruments BI-200 SM instrument (Holtsville, NY, USA). A Tristar 3000 analyzer

(Micromeritics, Atlanta, GA, USA) was employed to collect N_2 adsorption/desorption isotherms.

Cell lines and cell culture.

MDA-MB-231 cells, RAW264.7 cells and HUVEC cells were sourced from the Cell Bank of the Chinese Academy of Sciences (Shanghai, China). The cells (1×10^5 /mL) were cultured in DMEM containing penicillin-streptomycin (100 U mL^{-1}) and fetal bovine serum (10% v/v). Cultures were maintained in a 5% CO_2 humidified incubator at 37 ℃.

In vitro cellular uptake

Cells (MDA-MB-231 cells and RAW264.7) were charged in 35 mm confocal dishes (8×10^5 cells per dish) and incubated for 24 h. The culture medium was aspirated, and the cells cultured for 2 h in 2 mL of serum-free medium supplemented with DOX, DOX@MPDA NPs and PLTM-DOX@MPDA NPs. Experiments were matched to ensure an equivalent DOX concentration of 5 μg mL^{-1} in each case. Some experimental groups were treated witho an 808 nm laser (1.5 W cm^2) for 5 min midway through the 2 h incubation. After incubation, the cells were fixed with an aqueous solution of glutaraldehyde (2.5% w/v) at 4 ℃ for 15 min. They cells were next stained with Hoechst33342 for 30 min in the dark, and washed twice with PBS. Finally, images were obtained on a confocal laser-scanning microscope (CLSM; FV1000 microscope; Olympus, Tokyo, Japan).

NP uptake by MDA-MB-231 cellswas quantified by flow cytometry. Cells were loaded into 6-well plates (2 mL, 1×10^6 cells per well), and cultured for 24 hours. After this the medium was replaced with 2 mL of serum-free medium supplemented with DOX, DOX@MPDA NPs or PLTM-DOX@MPDA NPs (again ensuring an equivalent DOX concentration of 5 μg mL^{-1}). After incubation at 37 °C for 4 h, the cells were collected and uptake was measured with a FACScan analyzer (Becton-Dickinson, Franklin, CA, USA).

In vitro cytotoxicity

A suspension of MDA-MB-231 cells (10^5 cells/mL) was loaded into a 96-well plate (200 μL per well), and cultured for 12 h. Next, the medium was removed. Fresh culture medium containing varied concentrations of DOX, PLTM-DOX@MPDA NPs, PLTM-DOX@MPDA NPs (1 ,2, 4, 8, 16 and 20 μg/mL DOX) was added to each well to replace the original medium and the plate again incubated for 24 h. The medium was then aspirated and 20 μL of MTT solution added to each well before another incubation step lasting 4 hours. After this, the MTT solution was removed and 100 μL of DMSO added to each well. After shaking for 15 min, the optical density (OD) at 490 nm was measured on a PowerWave XS microplate reader (Bio-Tek, Winooski, VT, USA). Three independent experiments were performed with five replicates in each. Cell viability is calculated as= OD experimental group / OD control group × 100%.

In order to verify the results of MTT assays, Calcein-AM/PI staining was carried out. MDA-MB-231 cells (10^5 cells/mL) were loaded into 24-well plates (2 mL per well), incubated for 24 h, and then treated as for the MTT experiments. After incubation with the test formulations, the cells were stained with Calcein-AM and PI and imaged with a TE-2000U inverted phase contrast microscope (Olympus, Tokyo, Japan).

Animal tumor model

Nude mice (15~20 g, female) were provided by the Shanghai SLAC Experimental Animal Center (Shanghai, China). All animal experiments were performed according to international best practice and following approval from the Institutional Animal Care and Use Committee of Donghua University. 1×10^6 MDA-MB-231 cells in 100 μL of PBS (pH =7.4) was injected subcutaneously to the right flank of nude mice to establish a tumor model. The tumor volume was calculated as

length/2 × width^2.

Pharmacokinetics and biodistribution

In pharmacokinetics studies, free DOX or PLTM-DOX@MPDA were injected intravenously in nude mice (n=3 in each group) at a DOX dose of 5 mg/kg. Periodically, 15 μL of blood was collected from the ophthalmic vein, . centrifuged (3000 rpm, 4 ℃, 15 min), and the concentration of DOX determined at 490 nm using HPLC (ZORBAX SB-C18 column; Agilent Technologies, Santa Clara, CA, USA). A methanol/ acetonitrile/ammonium dihydrogen phosphate mixture (50: 22: 28 v/v) comprised the mobile phase (flow rate:1 mL min^{-1}).

To explore biodistribution, nude mice were randomly divided into two groups (n=6 in each). Free DOX or PLTM-DOX@MPDA was injected intravenously at a dose of 5 mg/kg. 24 h later, the mice were sacrificed and the hearts, livers, spleen, lungs, kidneys and tumors were collected. After weighing, digesting, diluting and filtering, the content of DOX was determined by HPLC as above.

In vivo anti-tumor efficacy and photothermal imaging

When the tumor volume reached ca. 100 mm^3, tumor-bearing mice were randomly divided into 5 groups (n = 6 in each). These were then subject to 5 different treatments: (1) saline (control), (2) MPDA+NIR, (3) free DOX, (4) PLTM-DOX@MPDA, (5) PLTM-DOX@MPDA+NIR. Each mouse in the treatment groups was injected intravenously with the appropriate formulation at a dose of 5 mg DOX per kg every 2 days for 14 days. The mice in the NIR groups were irradiated at the tumor site with an 808 nm laser (1.0 W cm^2 for 10 min) 12 hours after injection. Thermal images of the mice were recorded by infrared thermography (FLIRE 50 camera, Fluke, Everett, WA, USA) during the treatment. The mice's body weights were measured every 2 days. After 14 days of treatment, the mice were sacrificed and the major organs and tumor recovered. Tumor tissue was

sectioned in paraffin, and subjected to hematoxylin and eosin (H&E) and TdT-mediated dUTP-biotin nick end labeling (TUNEL) staining. The major organs were additionally stained with H&E.

Statistical analysis

Data for all experiments are given as mean ± standard deviation (SD). All experiments were carried out at least in triplicate. Statistical significance was determined using a student's t-test, and significant differences denoted as (*) $P < 0.05$, (**) $P < 0.005$ and (***) $P < 0.001$.

RESULTS AND DISCUSSION

Synthesis of PLTM- DOX @ MPDA

Dopamine is known to self-polymerize around F127 micelles in an aerobic environment to form PDA[18]. A mesoporous structure can be generated as a result of to π-π stacking interactions between PDA and the template TMB. The IR spectrum of the PDA particles generated is shown in Figure S1 (Supplementary Information). Peaks may be observed at 1635 cm^{-1} (C=C stretching), and 3220 cm^{-1} (O-H and N-H stretching) These features are consistent with literature reports for PDA[24, 31]. A TEM image of the particles is presented in Figure 2(a,b) and shows them to have a roughly spherical morphology and irregular mesoporous structure. Nitrogen adsorption-desorption data (Figure 2c) revealed a wide capillary condensation with an H4 hysteresis ring at a relative pressure of 0.4 to 0.8, and a wide capillary condensation with an H3 hysteresis loop at relative pressure of 0.8 to 1.0. It can thus be concluded that nitrogen adsorption-desorption by MPDA NPs follows a type IV isotherm. The Barrett-Joiner-Halenda (BJH) model was applied to study the pore size distribution of the MPDA NPs (Figure 2d). The presence of a 46 nm peak and wide pore size distribution demonstrates the MPDA particles to have an irregular mesoporous structure, which is consistent TEM images.

The drug loading was quantified by UV-vis spectroscopy (Figure S2). The DOX@MPDA NPs exhibit a distinctive absorbance peak arising from DOX at 490 nm. This confirms successful loading. The drug loading of DOX is calculated to be 38.6 ± 1.8% w/w, and the encapsulation efficiency is 98.9 ± 0.4%. A TEM image of the PLTM-DOX@MPDA NPs is presented in Figure 2e. The mesoporous structure is much harder to see here than in Figure 2a,b, and there is a shadow around the particles. This is thought to correspond to the PLTM wrapping. Successful loading of DOX and coating is also indicated by DLS, where the particle size increases slightly after each step (Figure 2f). The hydrodynamic diameter of the MPDA NPs is about 164 nm, while after loading with DOX the average particle size is 172 nm. The hydrodynamic diameter of the final particles coated with the PLTM is 184 nm. It is important to note that the particle size of the material remains below 200 nm, which means that there is the potential for "double targeting" of a tumor through both the EPR effect and active targeting. Further analysis in terms of zeta potential (Figure 2g) shows that the potential of MPDA NPs is -33.4 ± 0.6 mV. After the addition of DOX, the potential of DOX@MPDA NPs is -21.9 ± 0.5 mV. The clear change of potential supports the fact that DOX was successfully loaded onto the MPDA NPs. Finally, the potential decreased significantly after wrapping with the platelet membrane.

Western blotting results are depicted in Figure 2h. They reveal that the PLTM-DOX@MPDA NPs displayed the same protein bands as the platelet membrane. Quantitative analysis of these data (Figure 2i) revealed that there are reduced concentrations of CD41, CD47 and P-selectin in the coated NPs as compared to the PLTM. All of these findings indicate successful fabrication of the target drug delivery system.

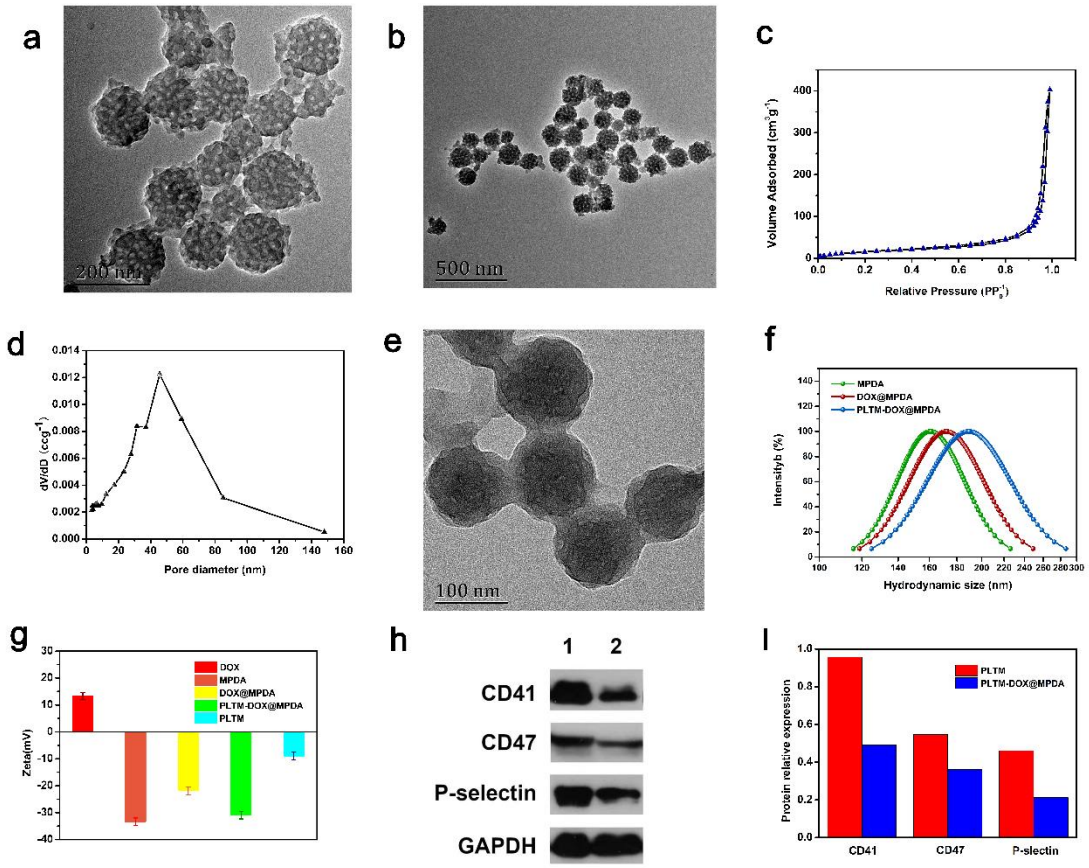

Figure 2. (a,b) TEM images of (a, b) MDA NPs; (c) N_2 adsorption/desorption isotherms of MPDA NPs and (d) the corresponding pore-size distribution curve; (e) TEM image of PLTM-DOX@MPDA NPs; (f) DLS plots for the different particles; (g) zeta potentials (mean±S.D.,n=3); (h) western blots showing the major platelet membrane protein bands of (1) PLTM and (2) PLTM-DOX@MPDA NPs; (i) quantitative analysis of the data in (h).

Photothermal effects and drug release

The PTT properties of the NPs were explored with NIR laser irradiation. Using laser irradiation at 1.5 W/cm^2, the temperature of the PLTM-DOX@MPDA suspension increases with time in a concentration-dependent manner. At a concentration of 1000 μg/mL, the suspension temperature was raised from 22.8 ℃ to 52.6 ℃ over 5 minutes, while a PBS negative control only increased by 3.9 ℃ (Figure 3a). Analogous observations are seen when the laser power is increased: a 500 μg/mL suspension of PLTM-DOX@MPDA increased from 24.5 to 85.4 ℃ when exposed to 2.5 W/cm^2 irradiation for 5 minutes (Figure 3b). Photothermal images (Figure 3c) are consistent with these findings. The PLTM-DOX@MPDA NPs thus have potent photothermal properties. Over 5 on-off

cycles, there is no noticeable change in the temperature vs time plots, indicating the formulation to have good stability and reusability (Figure 3d). The photothermal conversion efficiency (PTCE) of PLTM-DOX@MPDA NPs was determined to be 42% (Figure 3d). This is consistent with values previously reported for PDA[51] and higher than other PTAs such as ICG (21.2%)[4] and Ce6 (35.4%).[5]

The release of DOX was studied at pH values of pH=5.0 or 7.4. The effect of laser irradiation was also probed. At the physiological pH (7.4) without near infrared irradiation, the cumulative release of DOX was approximately 18.4% after 24 hours (Figure 3f), much lower than at pH 5.0 (58.2%). When pH 5.0 conditions were accompanied by laser irradiation, the cumulative release reached 84.7%. The NPs thus are able to respond to both pH and laser stimulation. This is due to the fact that MPDA and DOX can be covalently bound together via the formation of surface Schiff base groups (see Figure S3). A lower pH increases the protonation of amino groups of DOX and increases its hydrophilicity, thus increasing the release of DOX. The temperature rise initiated upon absorption of near-infrared light accelerates this process. The higher temperature may also destroy the platelet membrane structure, reducing the steric hindrance to DOX exiting the MPDA mesoporous structure, and increasing drug release.

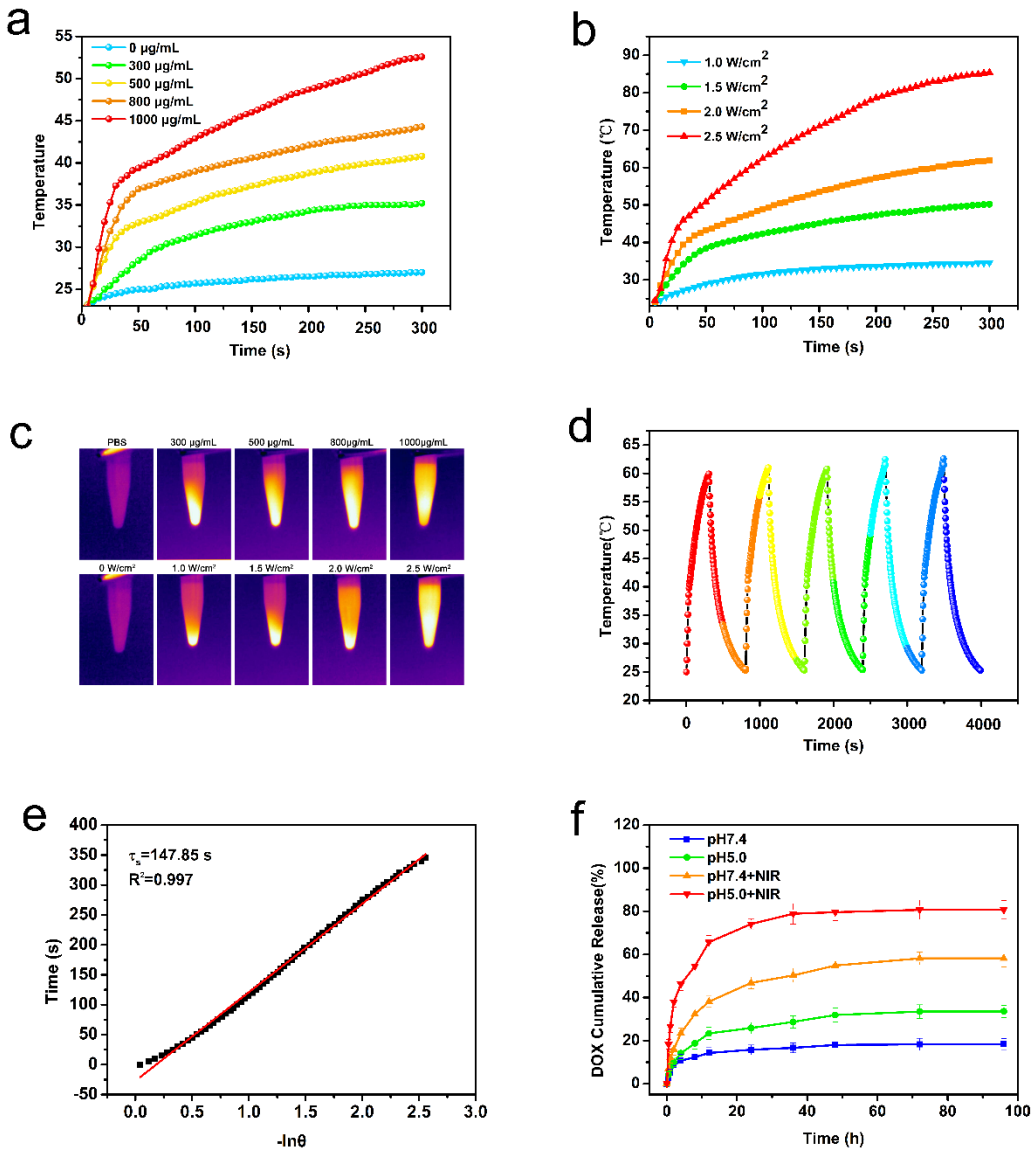

Figure 3. PTT data and drug release data for PLTM-DOX@MPDA suspensions. (a) Temperature variation curves obtained at various concentrations during 5 min irradiation with a laser power density of 1.5 W cm^{-2}, (mean ± S.D.; n = 3). (b) Temperature variation curves of 0.5 mg mL^{-1} suspensions at varied power densities over 5 min, (mean ± S.D.; n = 3). (c) Photothermal images showing representative images from (a) and (b) after 5 min irradiation. (d) Temperature changes for a 0.8 mg mL^{-1} suspension irradiated at 2 W cm^{-2} for five on–off cycles. (e) Linear regression between cooling time and –ln θ (1 mg mL^{-1} suspension irradiated at 2 W cm^{-2} for 5 min). (f) In vitro DOX release recorded over 96 h (mean ± S.D.; n = 3)

Cellular uptake

Cellular uptake of the NPs by MDA-MB-231 cells was next investigated using CLSM (Figure 4). The DOX fluorescence inside MDA-MB-231 cells treated with the PLTM-DOX@MPDA NPs is clearly greater than when the cells are given free DOX. The reason for this is that the structure of

the platelet membrane is similar to that of the cell membrane. Since the cell membrane has some degree of fluidity, cells can easily take up particles with lipid bilayers at their surface[52]. Further, there is P-selectin expressed on the platelet membrane, which can bind to the CD44 receptor on the cancer cell membrane and increase uptake. The DOX fluorescence signal is stronger still when the cells are treated with PLTM-DOX@MPDA augmented with laser irradiation, possibly due to slight damage to the cell membrane being caused by the elevated temperatures generated under laser irradiation.

The uptake of the formulations by RAW264.7 macrophage cells was also studied. Contrasting results to those with MDA-MB-231 cells were obtained (Figure 4). With RAW264.7 cells, the DOX fluorescence is stronger when the cells are given DOX@MPDA NPs, while the signal in the group treated with PLTM-DOX@MPDA is very weak. This is because the immunomodulatory protein CD47 on the surface of PLTM can prevent macrophage phagocytosis[49].

In order to further study PLTM-DOX@MPDA NPs uptake by cells, flow cytometry was used for quantitative analysis. The results are given in Figure S4, and it is clear that the uptake of PLTM-DOX@MPDA NPs group is greater than the free DOX group.

Hoechst 33342
DOX
Merge
Control
DOX@MPDA
PLTM-DOX @MPDA
PLTM-DOX @MPDA+NIR
Control
DOX@MPDA
PLTM-DOX @MPDA
MDA-MB-231 Cells
RAW264.7 Cells

Figure 4. Confocal fluorescence images of RAW264.7 and MDA-MB-231 cells treated with free DOX, DOX@MPDA NPs or PLTM-DOX@MPDA NPs for 4h. Representative images from three independent experiments are presented.

Cytotoxicity analysis

The cytotoxicity of the formulations was studied using the MTT method in MDA-MB-231 and HUVEC cells. The results showed that the relative cell viability of MDA-MB-231 cells incubated with PLTM-DOX@MPDA NPs for 24 hours decreased significantly compared to free DOX and other groups (Figure 5a), and showed a concentration-dependent trend. The survival rate of cancer cells treated with PLTM-DOX@MPDA NPs at 20 μg/mL and laser irradiation was only 14.3%. This value is significantly lower than the survival rate of cells given with the same concentration of free DOX (71.6%), indicating that photothermal therapy combined with chemotherapy leads to a synergistic cytotoxic effect. In contrast, the survival rates of healthy HUVEC cells (Figure 5b) treated with MPDA NPs, PLTM-MPDA NPs and PLTM-DOX@MPDA NPs are higher than 80%, indicating that all the NPs have excellent biocompatibility.

The effect of synergistic therapy using the PLTM-DOX@MPDA NPs on MDA-MB-231 cells can be shown visibly using Calcein AM/PI staining (Figure 5c). Increasing numbers of cells exhibiting red fluorescence (representing apoptosis) are visible when MDA-MB-231 cells are treated with the various NPs. Almost all MDA-MB-231 cells treated with PLTM-DOX@MPDA NPs and laser irradiation are stained red, indicating that they are dead. This is fully consistent with the MTT data.

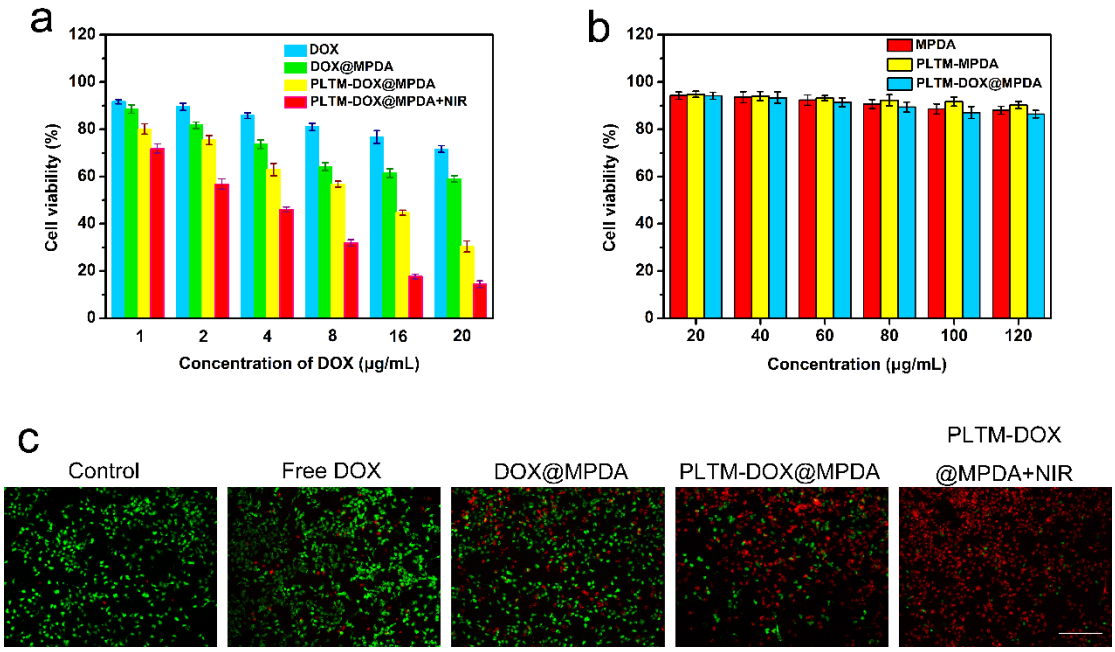

Figure 5. Relative cell viabilities of (a) MDA-MB-231 cells after incubation with the NP materials at different DOX concentrations, with or without laser irradiation (808 nm, 1.0 W cm^{-2}, 5 min) and (b) HUVEC cells after incubation with selected formulations at various concentrations for 12 h. In both cases, data are normalized to the untreated cells negative control, which is set to have a viability of 100%. (mean ± S.D.; n = 15; 3 independent experiments with 5 replicates in each) .(c) Fluorescence images of MDA-MB-231 cells costained with calcein AM/PI after different treatments. Scale bar: 100μm.

In vivo photothermal imaging

One of the benefits of PTT is that local changes in temperature can be used for imaging[15, 26]. The tumor-model mice were subjected to thermal imaging under 808 nm near-infrared light after treatment (Figure 6a). The temperature of the laser irradiation site in the control group injected with saline did not increase significantly, and was only slightly higher (ΔT=3.4℃) than the normal body temperature after irradiation for ten minutes. The temperature of the tumor site of the PLTM-DOX@MPDA NPs group increased significantly after laser irradiation, by about 20 ℃ (from 31 to 51 ℃). This both allows the imaging of the tumor and should be effective in the killing of tumor cells.

Pharmacokinetics and biological distribution studies

The in vivo pharmacokinetics of both DOX in solution and PLTM-DOX@MPDANPs were quantified in nude mice (Figure 6b). The concentration of free DOX in the plasma decreased to an undetectable level 24 hours after injection, while for the PLTM-DOX@MPDA NPs group the DOX concentration remained at ca. 2.82 μg/mL after the same time. Such a long blood circulation time should aid the NPs in accumulating effectively in the tumor.

Mice were sacrificed after 24 hours to investigate the biodistribution of the drug (Figure 6c). The amount of DOX in the tumors of mice treated with PLTM-DOX@MPDA NPs was greater than that in the other organs, suggesting the NPs show tumor selectivity. This arises as a result of the EPR effect and the active targeting of P-selectin to CD44 receptors on the membrane of the MDA-MB-231 cells, which permits them to avoided being captured by the reticuloendothelial system. A large amount of DOX was found in the kidneys and livers of mice given the NP formulations. This suggests that PLTM-DOX@MPDA NPs which do not reach the tumor can quickly be cleared from the body by standard metabolic routes. The accumulation of NPs in the liver presumably arises because of uptake by the mononuclear phagocytic system. The NPs present in the kidney are expected to be directly filtered from the blood[53].

In vivo antitumor efficacy

The efficacy and systemic toxicity of PLTM-DOX@MPDA NPs were studied in an MDA-MB-231 murine model. During treatment, the volume of the tumors (Figure 6d) and the weight of the nude mice were monitored every two days. In all cases, the tumor volume was seen to become greater with time. The control saline group showed the fastest and greatest increase in volume. The smallest increase was noted with the PLTM-DOX@MPDA NPs + NIR group, indicating the

synergistic therapy has a significant therapeutic effect on MDA-MB-231 tumors. This is also shown through visual inspection of the tumors excised at the end of the experiment (Figure 6e).

Body weight measurements (Figure 6f) show a general increase with time, likely attributable to tumor growth. The DOX group shows an initial increase in weight and then a reduction, indicating that DOX has off-target side effects causing weight loss even as the tumor grows. The PLTM-DOX@MPDA groups (with and without NIR irradiation) show minimal increases in weight: this suggests that there are minimal side-effects occurring here.

TUNEL and H&E staining (Figure 6e) were performed on tumor samples after the end of the experiment. H&E staining revealed significant amounts of apoptosis in the tumors of animals treated with DOX formulations, particularly those receiving PLTM-DOX@MPDA NPs. This is much less evident in the control and other treatment groups. Similar to the results of H&E staining, a high level of apoptotic cells (green) is visible in TUNEL staining with the PLTM-DOX@MPDA NPs+NIR group, but is not seen after the other treatments. This shows that the combination of photothermal therapy and chemotherapy of PLTM-DOX @ MPDA NPs has a potent therapeutic effect on tumor.

Finally, the major organs (heart, liver, spleen, lung and kidney) were analyzed by H&E staining (Figure S5), which revealed that the morphology of the organs in each group was normal, and there was no notable damage, inflammation, or apoptosis. The results show that the nanoparticles have good tumor targeted therapeutic effect and do not result in damage to healthy organs. Hence, the PLTM-DOX@MPDA NPs can be said to have good biocompatibility.

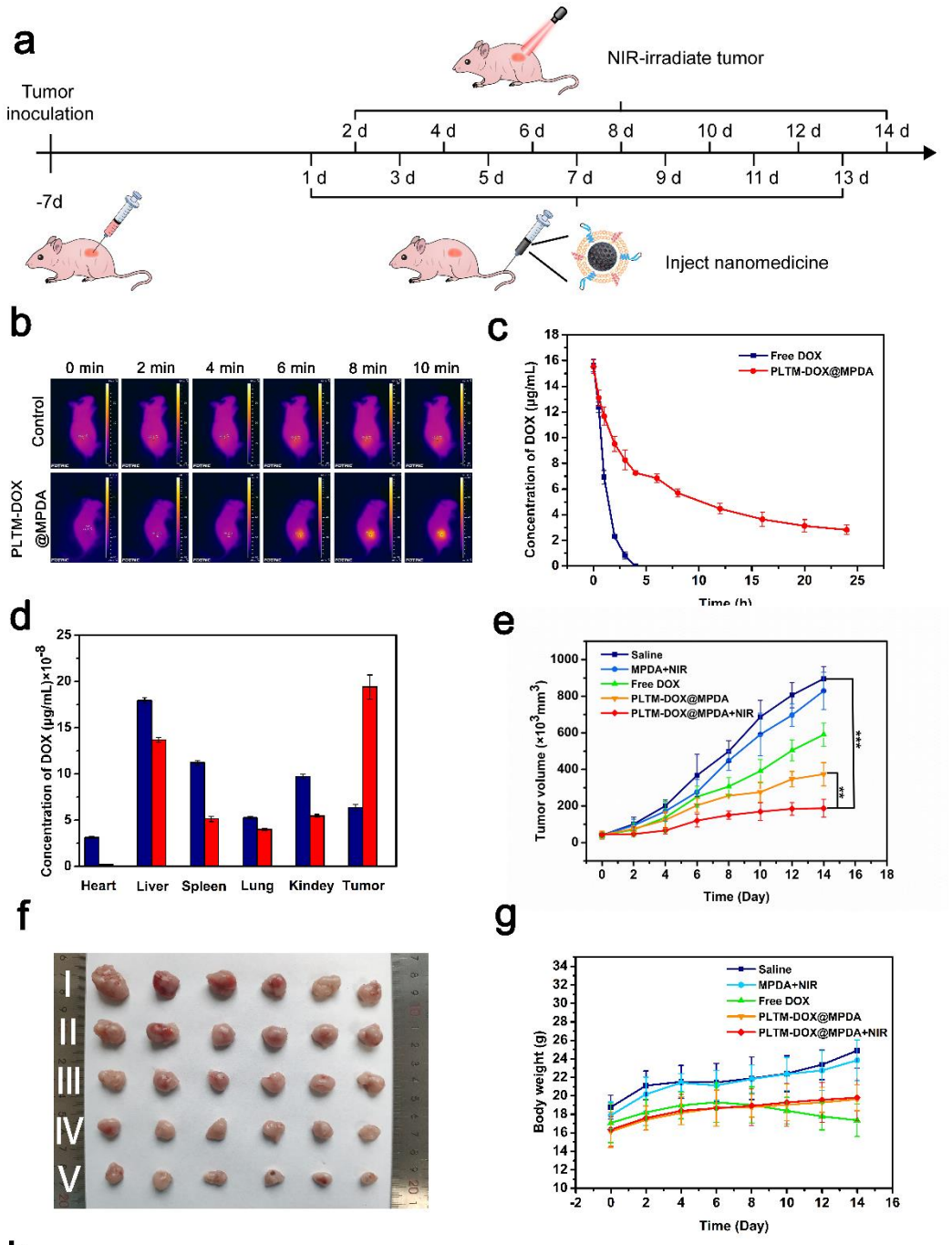
a
NIR-irradiate tumor
Tumor inoculation
2 d
4 d
6 d
8 d
10 d
12 d
14 d
1 d
3 d
5 d
7 d
9 d
11 d
13 d
-7d
Inject nanomedicine
b
0 min
2 min
4 min
6 min
8 min
10 min
Control
PLTM-DOX @MPDA
c
Free DOX
PLTM-DOX@MPDA
Concentration of DOX (μg/mL)
Time (h)
d
Concentration of DOX (μg/mL)×10-8
Heart
Liver
Spleen
Lung
Kindey
Tumor
e
Saline
MPDA+NIR
Free DOX
PLTM-DOX@MPDA
PLTM-DOX@MPDA+NIR
Tumor volume (×10³mm³)
Time (Day)
***
**
f
I
II
III
IV
V
g
Saline
MPDA+NIR
Free DOX
PLTM-DOX@MPDA
PLTM-DOX@MPDA+NIR
Body weight (g)
Time (Day)
h
Control
MPDA+NIR
Free DOX
PLTM-DOX@MPDA
PLTM-DOX@MPDA +NIR
H&E Staining
TUNEL Assay
50 μm
50 μm

Figure 6. (a) A schematic depicting the chemo- photothermal combined therapy approach; (b) Thermal images of MDA-MB-231 tumor-bearing mice treated with PBS or PLTM-DOX@MPDA NPs and 808 nm laser irradiation at 1.0 Wcm^{-2} for 5 min. (c) Plasma concentration vs time for free DOX and PLTM-DOX@MPDA NPs in nude mice (n = 3, mean ± S.D.). (d) Ex vivo DOX concentration in the different organs after 24 h. (mean ± S.D.; n = 3) (e) Tumor volume data recorded during *in vivo* experiments (mean ± S.D.; n = 6). **P< 0.01, and ***P< 0.001 (*cf.* saline control). (f) Digital images of tumor tissues removed after 14 days of treatment with (I) saline (control), (II) MPDA+NIR (III) free DOX, (IV) PLTM-DOX@MPDA(V) PLTM-DOX@MPDA (g) Body weights recorded during *in vivo* experiments (mean ± S.D.; n = 6). (h) Histology images showing tumor sections stained with H&E and TUNEL . Scale bars: 50 μm.

Compared with other MPDA-based nano-drug delivery systems, the PLTM modified materials prepared in this paper have a number of advantages. In a previous report, Xing et al modified MDPA with d-α-tocopheryl polyethylene glycol 1000 succinate (TPGS), employing the TPGS with the aim of targeting mitochondrial organelles and thus improving the therapeutic effect of the NPs[29]. However, this intracellular organelle targeting is only efficient if the NPs reach the cell in the first place, and in general nano-carriers can only passively target the tumor site through the EPR effect. Other cell membrane biomimetic delivery systems have been reported, such as that from Wan et al., who prepared erythrocyte membrane coated nanoparticles[44]. These make use of the erythrocyte's biocompatibility, low immunogenicity and long circulation time in vivo to enhance the anti-tumor effect of nano-carriers. However, the RBCM lacks the ability for active targeting to tumor cells. PLTM not only has the above advantages, but also provides active targeting. The latter arises because there is specific binding of P-selectin on the PLTM to CD44 receptors, which are overexpressed by the target tumor cells. These concepts of CD47-mediated phagocytosis avoidance and P-selectin-CD44 complementarity have been documented to be important in the progression and targeting of human tumors.

CONCLUSIONS

In this work, a targeted drug delivery system for cancer is developed. This was generated by first preparing mesoporous polydopamine (MPDA) nanoparticles, and loading them with the chemotherapeutic doxorubicin (DOX). The formulation was then coated with the platelet membrane (PLTM) to yield biomimetic particles. These particles have small sizes (< 200 nm), potent photothermal properties, and show accelerated drug release in conditions mimicking the tumor microenvironment. Uptake by cancerous cells is promoted by the PLTM coating, while phagocytosis by macrophage cells is inhibited. Thus, the formulation is able to target cancer cells both through active and passive targeting. The PLTM-DOX@MPDA NPs are shown to be highly effective in reducing tumor volume in a murine cancer model, and to have extended pharmacokinetics over the free drug. They further display high biocompatibility, with no observable off-target effects.

ASSOCIATEDCONTENT

Supporting Information.

Figure S1. Material characterization, FTIR spectrum of MPDA NPs. It is proved that the main functional group of MPDA is the same as dopamine.

Figure S2. Material characterization, UV–vis absorption spectra of selected nanoparticles. It is proved that the drug is loaded successfully.

Figure S3. Schematic diagram of the Schiff base reaction between MPDA and DOX, Explained the principle of drug loading and pH sensitively release.

Figure S4. Flow cytometry data for MDA-MB-231 cells incubated with (a) PBS, (b) free DOX, (c) DOX@MPDA (d) PLTM-DOX@MPDA and (e) PLTM-DOX@MPDA+NIR. Flow cytometry was used to detect the DOX uptake of cancer cells in different nano-drug loading systems, so as to judge the active targeting ability of nano-drug loading systems.

Figure S5.H&E stained images of the main organs of nude mice, the results showed that the degree of tissue injury after PLTM-DOX@MPDA+NIR treatment was significantly lower than that of free DOX group, which proved that of the nano-carrier was biological safe.

Figure S6-S8. Full membrane WB image of CD41、CD47 and P-selectin

Acknowledgements

This investigation was supported by the Biomedical Textile Materials “111 Project” of the Ministry of Education of China (No. B07024) and grant 16410723700 awarded by the Science and Technology Commission of Shanghai Municipality.

Declaration of Competing Interest

The authors declare that they have no known competing financial interests or personal relationships that could have appeared to influence the work reported in this paper.

REFERENCES

1. Lin, X.; Fang, Y.; Tao, Z.; Gao, X.; Wang, T.; Zhao, M.; Wang, S.; Liu, Y., Tumor-Microenvironment-Induced All-in-One Nanoplatform for Multimodal Imaging-Guided Chemical and Photothermal Therapy of Cancer. *ACS Appl Mater Interfaces* **2019,** *11* (28), 25043-25053.
2. Wang, Y.; Meng, H. M.; Li, Z., Near-infrared inorganic nanomaterial-based nanosystems for photothermal therapy. *Nanoscale* **2021,** *13* (19), 8751-8772.
3. Hu, D.; Liu, C.; Song, L.; Cui, H.; Gao, G.; Liu, P.; Sheng, Z.; Cai, L., Indocyanine green-loaded polydopamine-iron ions coordination nanoparticles for photoacoustic/magnetic resonance dual-modal imaging-guided cancer photothermal therapy. *Nanoscale* **2016,** *8* (39), 17150-17158.
4. Cao, D.; Li, H.; Luo, Y.; Feng, N.; Ci, T., Heparin modified photosensitizer-loaded liposomes for tumor treatment and alleviating metastasis in phototherapy. *Int J Biol Macromol* **2021,** *168*, 526-536.
5. Yang, X.; Wang, D.; Shi, Y.; Zou, J.; Zhao, Q.; Zhang, Q.; Huang, W.; Shao, J.; Xie, X.; Dong, X., Black Phosphorus Nanosheets Immobilizing Ce6 for Imaging-Guided Photothermal/Photodynamic Cancer Therapy. *ACS Appl Mater Interfaces* **2018,** *10* (15), 12431-12440.
6. Deng, L.; Guo, W.; Li, G.; Hu, Y.; Zhang, L. M., Hydrophobic IR780 loaded sericin nanomicelles for phototherapy with enhanced antitumor efficiency. *Int J Pharm* **2019,** *566*, 549-556.
7. Dong, Z.; Gong, H.; Gao, M.; Zhu, W.; Sun, X.; Feng, L.; Fu, T.; Li, Y.; Liu, Z., Polydopamine Nanoparticles as a Versatile Molecular Loading Platform to Enable Imaging-guided Cancer Combination Therapy. *Theranostics* **2016,** *6* (7), 1031-42.
8. Deng, X.; Liang, H.; Yang, W.; Shao, Z., Polarization and function of tumor-associated macrophages mediate graphene oxide-induced photothermal cancer therapy. *J Photochem Photobiol B* **2020,** *208*, 111913.
9. Zheng, T.; Li, G. G.; Zhou, F.; Wu, R.; Zhu, J. J.; Wang, H., Gold-Nanosponge-Based Multistimuli-Responsive Drug Vehicles for Targeted Chemo-Photothermal Therapy. *Adv Mater* **2016,** *28* (37), 8218-8226.
10. Li, Y.; Liu, Z.; Hou, Y.; Yang, G.; Fei, X.; Zhao, H.; Guo, Y.; Su, C.; Wang, Z.; Zhong, H.; Zhuang, Z.; Guo, Z., Multifunctional Nanoplatform Based on Black Phosphorus Quantum Dots for Bioimaging and Photodynamic/Photothermal Synergistic Cancer Therapy. *ACS Appl Mater Interfaces* **2017,** *9* (30), 25098-25106.
11. Chen, G.; Roy, I.; Yang, C.; Prasad, P. N., Nanochemistry and Nanomedicine for Nanoparticle-based Diagnostics and Therapy. *Chem Rev* **2016,** *116* (5), 2826-85.
12. Wang, S.; Zhao, X.; Wang, S.; Qian, J.; He, S., Biologically Inspired Polydopamine Capped Gold Nanorods for Drug Delivery and Light-Mediated Cancer Therapy. *ACS Appl Mater Interfaces* **2016,** *8* (37), 24368-84.
13. Mrowczynski, R., Polydopamine-Based Multifunctional (Nano)materials for Cancer Therapy. *ACS Appl Mater Interfaces* **2018,** *10* (9), 7541-7561.
14. Zhao, H.; Chao, Y.; Liu, J.; Huang, J.; Pan, J.; Guo, W.; Wu, J.; Sheng, M.; Yang, K.; Wang, J.; Liu, Z., Polydopamine Coated Single-Walled Carbon Nanotubes as a Versatile Platform with Radionuclide Labeling for Multimodal Tumor Imaging and Therapy. *Theranostics* **2016,** *6* (11), 1833-43.
15. Zhang, L.; Su, H.; Cai, J.; Cheng, D.; Ma, Y.; Zhang, J.; Zhou, C.; Liu, S.; Shi, H.; Zhang, Y.; Zhang, C., A Multifunctional Platform for Tumor Angiogenesis-Targeted Chemo-Thermal Therapy Using Polydopamine-Coated Gold Nanorods. *ACS Nano* **2016,** *10* (11), 10404-10417.

16. Yuan, Z.; Lin, C.; He, Y.; Tao, B.; Chen, M.; Zhang, J.; Liu, P.; Cai, K., Near-Infrared Light-Triggered Nitric-Oxide-Enhanced Photodynamic Therapy and Low-Temperature Photothermal Therapy for Biofilm Elimination. *ACS Nano* **2020,** *14* (3), 3546-3562.
17. Liu, Y.; Ai, K.; Lu, L., Polydopamine and its derivative materials: synthesis and promising applications in energy, environmental, and biomedical fields. *Chem Rev* **2014,** *114* (9), 5057-115.
18. Lee, H.; Dellatore, S. M.; Miller, W. M.; Messersmith, P. B., Mussel-inspired surface chemistry for multifunctional coatings. *Science* **2007,** *318* (5849), 426-30.
19. Ge, R.; Li, X.; Lin, M.; Wang, D.; Li, S.; Liu, S.; Tang, Q.; Liu, Y.; Jiang, J.; Liu, L.; Sun, H.; Zhang, H.; Yang, B., Fe3O4@polydopamine Composite Theranostic Superparticles Employing Preassembled Fe3O4 Nanoparticles as the Core. *ACS Appl Mater Interfaces* **2016,** *8* (35), 22942-52.
20. Zhang, Y.; Yin, X.; Yu, B.; Wang, X.; Guo, Q.; Yang, J., Recyclable Polydopamine-Functionalized Sponge for High-Efficiency Clean Water Generation with Dual-Purpose Solar Evaporation and Contaminant Adsorption. *ACS Appl Mater Interfaces* **2019,** *11* (35), 32559-32568.
21. Shao, M.; Chang, C.; Liu, Z.; Chen, K.; Zhou, Y.; Zheng, G.; Huang, Z.; Xu, H.; Xu, P.; Lu, B., Polydopamine coated hollow mesoporous silica nanoparticles as pH-sensitive nanocarriers for overcoming multidrug resistance. *Colloids Surf B Biointerfaces* **2019,** *183*, 110427.
22. Wang, Z.; Zou, Y.; Li, Y.; Cheng, Y., Metal-Containing Polydopamine Nanomaterials: Catalysis, Energy, and Theranostics. *Small* **2020,** *16* (18), e1907042.
23. Zhang, C.; Zhao, X.; Guo, S.; Lin, T.; Guo, H., Highly effective photothermal chemotherapy with pH-responsive polymer-coated drug-loaded melanin-like nanoparticles. *Int J Nanomedicine* **2017,** *12*, 1827-1840.
24. Song, Y.; Zhu, P.; Xu, Z.; Chen, J., Dual-Responsive Dual-Drug-Loaded Bioinspired Polydopamine Nanospheres as an Efficient Therapeutic Nanoplatform against Drug-Resistant Cancer Cells. *ACS Applied Bio Materials* **2020,** *3* (9), 5730-5740.
25. Chen, F.; Xing, Y.; Wang, Z.; Zheng, X.; Zhang, J.; Cai, K., Nanoscale Polydopamine (PDA) Meets pi-pi Interactions: An Interface-Directed Coassembly Approach for Mesoporous Nanoparticles. *Langmuir* **2016,** *32* (46), 12119-12128.
26. Wu, D.; Zhou, J.; Chen, X.; Chen, Y.; Hou, S.; Qian, H.; Zhang, L.; Tang, G.; Chen, Z.; Ping, Y.; Fang, W.; Duan, H., Mesoporous polydopamine with built-in plasmonic core: Traceable and NIR triggered delivery of functional proteins. *Biomaterials* **2020,** *238*, 119847.
27. Wang, L.; He, Y.; He, T.; Liu, G.; Lin, C.; Li, K.; Lu, L.; Cai, K., Lymph node-targeted immune-activation mediated by imiquimod-loaded mesoporous polydopamine based-nanocarriers. *Biomaterials* **2020,** *255*, 120208.
28. Li, X.; Zou, Q.; Zhang, J.; Zhang, P.; Zhou, X.; Yalamarty, S. S. K.; Liang, X.; Liu, Y.; Zheng, Q.; Gao, J., Self-Assembled Dual-Targeted Epirubicin-Hybrid Polydopamine Nanoparticles for Combined Chemo-Photothermal Therapy of Triple-Negative Breast Cancer. *Int J Nanomedicine* **2020,** *15*, 6791-6811.
29. Xing, Y.; Zhang, J.; Chen, F.; Liu, J.; Cai, K., Mesoporous polydopamine nanoparticles with co-delivery function for overcoming multidrug resistance via synergistic chemo-photothermal therapy. *Nanoscale* **2017,** *9* (25), 8781-8790.
30. He, Y.; Niu, K.; Luo, L.; Li, L.; Cong, C.; Gao, D., Reduction and Protection: One-Step Synthesis of Polydopamine-Coated Silver Nanowires with Superior Biosafety for Cancer Treatment. *ACS Sustainable Chemistry & Engineering* **2019,** *7* (24), 20102-20106.
31. Wu, D.; Duan, X.; Guan, Q.; Liu, J.; Yang, X.; Zhang, F.; Huang, P.; Shen, J.; Shuai, X.; Cao,

Z., Mesoporous Polydopamine Carrying Manganese Carbonyl Responds to Tumor Microenvironment for Multimodal Imaging-Guided Cancer Therapy. *Advanced Functional Materials* **2019,** *29* (16) ,1900095.

32. Guan, Q.; Guo, R.; Huang, S.; Zhang, F.; Liu, J.; Wang, Z.; Yang, X.; Shuai, X.; Cao, Z., Mesoporous polydopamine carrying sorafenib and SPIO nanoparticles for MRI-guided ferroptosis cancer therapy. *J Control Release* **2020,** *320*, 392-403.

33. Seth, A.; Gholami Derami, H.; Gupta, P.; Wang, Z.; Rathi, P.; Gupta, R.; Cao, T.; Morrissey, J. J.; Singamaneni, S., Polydopamine-Mesoporous Silica Core-Shell Nanoparticles for Combined Photothermal Immunotherapy. *ACS Appl Mater Interfaces* **2020,** *12* (38), 42499-42510.

34. Battaglini, M.; Marino, A.; Carmignani, A.; Tapeinos, C.; Cauda, V.; Ancona, A.; Garino, N.; Vighetto, V.; La Rosa, G.; Sinibaldi, E.; Ciofani, G., Polydopamine Nanoparticles as an Organic and Biodegradable Multitasking Tool for Neuroprotection and Remote Neuronal Stimulation. *ACS Appl Mater Interfaces* **2020,** *12* (32), 35782-35798.

35. Gupta, B.; Poudel, B. K.; Ruttala, H. B.; Regmi, S.; Pathak, S.; Gautam, M.; Jin, S. G.; Jeong, J. H.; Choi, H. G.; Ku, S. K.; Yong, C. S.; Kim, J. O., Hyaluronic acid-capped compact silica-supported mesoporous titania nanoparticles for ligand-directed delivery of doxorubicin. *Acta Biomater* **2018,** *80*, 364-377.

36. Bertrand, N.; Wu, J.; Xu, X.; Kamaly, N.; Farokhzad, O. C., Cancer nanotechnology: the impact of passive and active targeting in the era of modern cancer biology. *Adv Drug Deliv Rev* **2014,** *66*, 2-25.

37. Li, L.; Liang, N.; Wang, D.; Yan, P.; Kawashima, Y.; Cui, F.; Sun, S., Amphiphilic Polymeric Micelles Based on Deoxycholic Acid and Folic Acid Modified Chitosan for the Delivery of Paclitaxel. *Int J Mol Sci* **2018,** *19* (10) ,3132.

38. Zhang, N.; Song, J.; Liu, Y.; Liu, M.; Zhang, L.; Sheng, D.; Deng, L.; Yi, H.; Wu, M.; Zheng, Y.; Wang, Z.; Yang, Z., Photothermal therapy mediated by phase-transformation nanoparticles facilitates delivery of anti-PD1 antibody and synergizes with antitumor immunotherapy for melanoma. *J Control Release* **2019,** *306*, 15-28.

39. Sun, M.; Guo, J.; Hao, H.; Tong, T.; Wang, K.; Gao, W., Tumour-homing chimeric polypeptide-conjugated polypyrrole nanoparticles for imaging-guided synergistic photothermal and chemical therapy of cancer. *Theranostics* **2018,** *8* (10), 2634-2645.

40. Fu, Z.; Williams, G. R.; Niu, S.; Wu, J.; Gao, F.; Zhang, X.; Yang, Y.; Li, Y.; Zhu, L. M., Functionalized boron nanosheets as an intelligent nanoplatform for synergistic low-temperature photothermal therapy and chemotherapy. *Nanoscale* **2020,** *12* (27), 14739-14750.

41. Shi, J.; Kantoff, P. W.; Wooster, R.; Farokhzad, O. C., Cancer nanomedicine: progress, challenges and opportunities. *Nat Rev Cancer* **2017,** *17* (1), 20-37.

42. Fang, R. H.; Kroll, A. V.; Gao, W.; Zhang, L., Cell Membrane Coating Nanotechnology. *Adv Mater* **2018,** *30* (23), e1706759.

43. Xu, C. H.; Ye, P. J.; Zhou, Y. C.; He, D. X.; Wei, H.; Yu, C. Y., Cell membrane-camouflaged nanoparticles as drug carriers for cancer therapy. *Acta Biomater* **2020,** *105*, 1-14.

44. Wan, G.; Chen, B.; Li, L.; Wang, D.; Shi, S.; Zhang, T.; Wang, Y.; Zhang, L.; Wang, Y., Nanoscaled red blood cells facilitate breast cancer treatment by combining photothermal/photodynamic therapy and chemotherapy. *Biomaterials* **2018,** *155*, 25-40.

45. Zhang, L.; Li, R.; Chen, H.; Wei, J.; Qian, H.; Su, S.; Shao, J.; Wang, L.; Qian, X.; Liu, B., Human cytotoxic T-lymphocyte membrane-camouflaged nanoparticles combined with low-dose irradiation: a new approach to enhance drug targeting in gastric cancer. *Int J Nanomedicine* **2017,** *12*,

2129-2142.
46. Cao, H.; Dan, Z.; He, X.; Zhang, Z.; Yu, H.; Yin, Q.; Li, Y., Liposomes Coated with Isolated Macrophage Membrane Can Target Lung Metastasis of Breast Cancer. *ACS Nano* **2016,** *10* (8), 7738-48.
47. Jin, J.; Bhujwalla, Z. M., Biomimetic Nanoparticles Camouflaged in Cancer Cell Membranes and Their Applications in Cancer Theranostics. *Front Oncol* **2019,** *9*, 1560.
48. Xu, L.; Gao, F.; Fan, F.; Yang, L., Platelet membrane coating coupled with solar irradiation endows a photodynamic nanosystem with both improved antitumor efficacy and undetectable skin damage. *Biomaterials* **2018,** *159*, 59-67.
49. Wang, H.; Bremner, D. H.; Wu, K.; Gong, X.; Fan, Q.; Xie, X.; Zhang, H.; Wu, J.; Zhu, L.-M., Platelet membrane biomimetic bufalin-loaded hollow MnO2 nanoparticles for MRI-guided chemo-chemodynamic combined therapy of cancer. *Chemical Engineering Journal* **2020,** *382*.
50. Shang, Y.; Wang, Q.; Wu, B.; Zhao, Q.; Li, J.; Huang, X.; Chen, W.; Gui, R., Platelet-Membrane-Camouflaged Black Phosphorus Quantum Dots Enhance Anticancer Effect Mediated by Apoptosis and Autophagy. *ACS Appl Mater Interfaces* **2019,** *11* (31), 28254-28266.
51. Liu, Y.; Ai, K.; Liu, J.; Deng, M.; He, Y.; Lu, L., Dopamine-melanin colloidal nanospheres: an efficient near-infrared photothermal therapeutic agent for in vivo cancer therapy. *Adv Mater* **2013,** *25* (9), 1353-9.
52. Zong, W.; Hu, Y.; Su, Y.; Luo, N.; Zhang, X.; Li, Q.; Han, X., Polydopamine-coated liposomes as pH-sensitive anticancer drug carriers. *J Microencapsul* **2016,** *33* (3), 257-62.
53. Du, B.; Yu, M.; Zheng, J., Transport and interactions of nanoparticles in the kidneys. *Nature Reviews Materials* **2018,** *3* (10), 358-374.

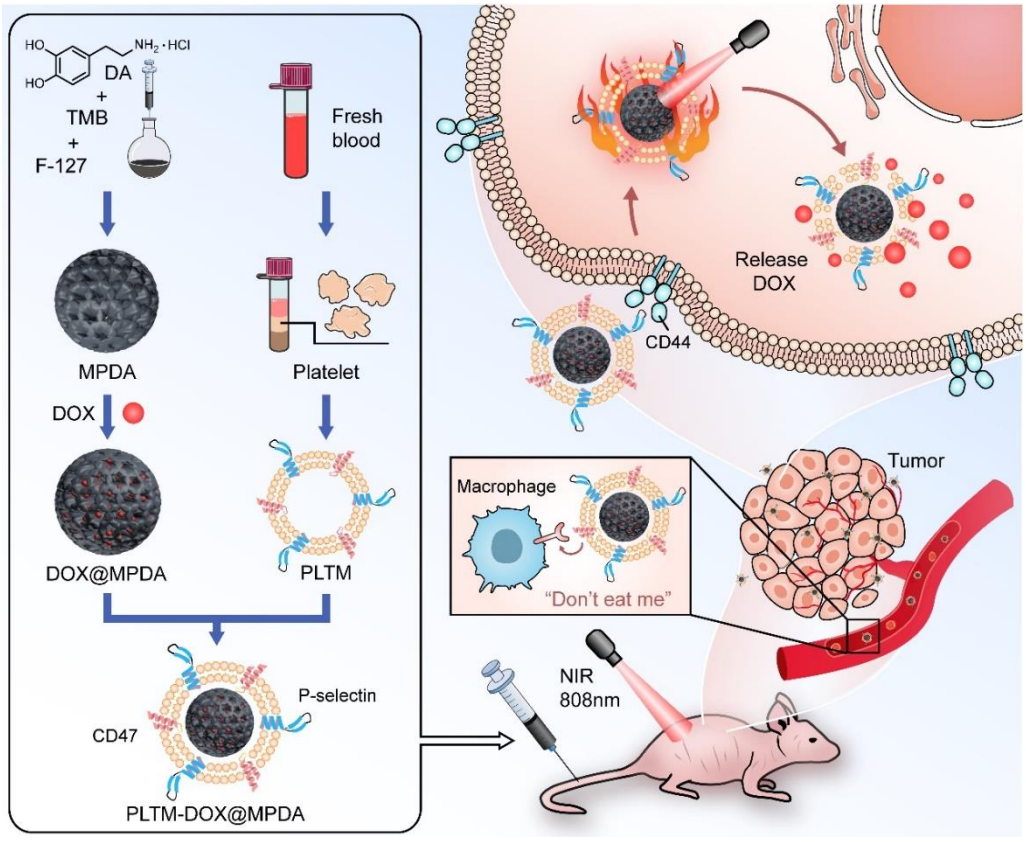

TOC graphic